Nanoscale

PAPER

View Article Online
View Journal | View Issue

Cite this: *Nanoscale*, 2017, **9**, 869

A flexible transparent colorimetric wrist strap sensor†

Ting Wang,[a,b,c] Yunlong Guo,[a] Pengbo Wan,*[a] Xiaoming Sun,[a] Han Zhang,*[b] Zhongzhen Yu[a] and Xiaodong Chen[c]

Received 21st October 2016,
Accepted 4th December 2016

DOI: 10.1039/c6nr08265c

www.rsc.org/nanoscale

A flexible, transparent, and portable wrist strap sensor device has been well developed from a hierarchical polydiacetylene/MoS_2 nanocomposite (PDA/MoS_2) film. MoS_2 with a nanoflake structure and chelation ability acts as a supporter for PDA films to enhance the porosity as well as the transparency of films, which increases the sensitivity, selectivity, and application potential of a PDA sensor. The PDA/MoS_2 film sensor shows a linear detection range for *N*,*N*-dimethylformamide (DMF) vapor from 0.01% to 4% with a visible blue to red color change detected by the naked eye, which is more sensitive than other organic vapors. Exploiting the high transparency, vivid color change, remarkable flexibility and reliability, a wearable wrist strap sensor device with visible DMF sensing ability is fabricated based on PDA/MoS_2 films, indicating their great potential for smart wearable devices.

Introduction

Smart flexible transparent films with sensing properties have been envisioned as promising components to be integrated into smart devices, such as wearable electronics, robots, health care electronics, and environment monitors.[1–3] With increasing environment pollution problems, environmental pollutant responsive sensors are highly desired, especially for readily absorbable gaseous pollutants, which can timely provide the concentration of pollutants at a specific place and thus give alarm signals for safety protection, once the environment is dangerous for the human body.[4–6] Solid powder-like gas-sensing materials deposited on ceramic tubes or inter-finger probes show great advantages when compared with laboratory-based analytical techniques such as gas chromatography mass spectrometry with reliable accuracy but bulk instrument and professional operations. Traditional gas sensors do not possess the required flexibility or transparency.[7] Recently, many efforts have been devoted to flexible transparent films with gaseous pollutant sensing properties based on semiconducting oxides, conducting polymers, and carbon materials, such as a flexible PbS quantum dot based film for an NO_2 sensor,[8] flexible CNT bundles on cellulosic films for a Cl_2 sensor,[9] and transparent CNT/PANI nanocomposites for an NH_3 sensor.[10] However, most of the reported gas sensors require high temperature in order to realize efficient gas adsorption on sensors, which calls for the implementation of a heating element, greatly hampering the flexibility, transparency, miniature, and especially the integration of sensors into portable and wearable devices. Moreover, the sensor responses are mostly based on gas-induced resistance changes and precise detection instruments are required.[11] Comparatively, a colorimetric sensor at room temperature capable of giving out a visually observable signal should partly avoid the above drawbacks and pose higher potential in practical applications.

Based on the tunable electronic and optical properties determined by the extended π-electron delocalization along backbones, conjugated polymers have been widely investigated for a broad spectrum of promising applications in optoelectronics and sensors.[12] Among them, polydiacetylene (PDA), as a typical conjugated polymer, has a unique property of color (blue-to-red) and fluorescence (non-to-fluorescent) changes under various external stimuli, such as temperature, pH, chemical or mechanical stress due to the deformation of the conjugated backbone induced by external stimuli.[13] Recently, novel PDA based sensors have been designed through modulating the structure of side chains, such as PDA with hygroscopic moieties into head groups for sweat pore mapping,[14] PDA-embedded PDMS films for hydrocarbon sensors,[15] and

[a]*State Key Laboratory of Organic-Inorganic Composites, College of Materials Science and Engineering, Beijing University of Chemical Technology, Beijing 100029, P.R. China. E-mail: pbwan@mail.buct.edu.cn*
[b]*SZU-NUS Collaborative Innovation Center for Optoelectronic Science & Technology, Key Laboratory of Optoelectronic Devices and Systems of Ministry of Education and Guangdong Province, Shenzhen University, Shenzhen 518060, China. E-mail: hzhang@szu.edu.cn*
[c]*School of Materials Science and Engineering, Nanyang Technological University, 50 Nanyang Avenue, Singapore 639798, Singapore*
†Electronic supplementary information (ESI) available: Characterization and performance results. See DOI: 10.1039/c6nr08265c

antibody-conjugated PDA vesicles for immunosensors,[16] all of which showed a visible naked-eye detectable signal without using an electronic detection instrument. However, PDA tends to aggregate and is therefore difficult to construct uniform films. To make the handling of colorimetric polymer sensors easier and overcome the drawback of aggregation of PDA films, the general solution is the immobilization of PDA onto the surfaces of membrane filters, silica microbeads, and glass fibers.[17] Even though advanced results have been obtained, transparency and flexibility of PDA based sensors still leave room for improvement, which allow for the enhancement of not only an aesthetic value but also versatility in the design and usage of devices.

Two-dimensional (2D) nanomaterials, including graphene and transition metal dichalcogenides (TMDCs), have drawn increasing attention due to their unique electronic and optical properties inherited from their dimensional advantages.[18–20] In particular, their 2D planar structure enables facile assembly into macroscopic frameworks with different macroscaled shapes, which can be used as ideal scaffolds with the desired flexibility and transparency for the incorporation of functional materials, such as nanoparticles and conjugated polymers.[21,22] Molybdenum disulfide (MoS_2), a typical TMDC with a nanosheet structure, is a semiconducting material with a tunable energy band-gap that sensitively depends on its layer number, as well as promising optical, catalytic, and gas sensing properties.[23] On the one hand, being a thin material with a 2D morphology of mechanical flexibility, optical transparency, and high surface area, an exfoliated MoS_2 nanosheet should be considered as an excellent candidate for flexible and transparent devices. On the other hand, the transition metal centers of metal dichalcogenides have been reported to strongly coordinate with atoms of lone electron pairs such as nitrogen atoms in polyaniline, which thus benefit the controllable growth of polymers onto the 2D nanosheet surfaces and decrease the aggregation of polymers.[24,25] Inspired by these, based on the possible chelation interaction between MoS_2 and the carboxyl group of PDA, rational design of hierarchical polydiacetylene/molybdenum disulfide nanocomposites (PDA/MoS_2) could incorporate the merits of MoS_2 into PDA based sensors, which renders the possibility of constructing flexible and transparent colorimetric gaseous sensors with high performance.

N,*N*-Dimethylformamide (DMF), a most commonly used solvent in industrial manufacture, has been suggested to induce hepatotoxicity, embryotoxicity, tumors, even carcinogenesis through skin contact and inhalation in various industries.[26,27] Due to the widespread use of DMF, a large number of people at risk, and complicated detection procedures, a rapid and facile sensor for DMF vapor is highly desirable.[28] It has been reported that 2D MoS_2 has a high affinity to N-containing gas species such as NH_3 and trimethylamine due to the interaction of the localized lone pair orbitals of the sulfur end units with donor-like analytes.[29–31] Synergistically combining the merits of MoS_2 and PDA, the present research study was targeted to construct a flexible and transparent sensor based on PDA/MoS_2 films for selectively monitoring DMF vapor, which has high potential to be integrated into wearable and portable devices.

Experimental

Materials

10,12-Pentacosadiynoic acid (PCDA) was purchased from Alfa Aesar. Bulk MoS_2 crystals were purchased from Sigma Aldrich. Polyethylene terephthalate (PET) films (125 μm) were purchased from Hui Zhixing Company (Hangzhou, China). All other reagents and solvents were of analytical grade and supplied by local commercial suppliers. Ultrapure water used in all experiments was supplied by using a Milli-Q system (Millipore).

Preparation of MoS_2

1 g MoS_2 bulk (99% purity, Sigma-Aldrich) was added to a mortar and ground with a pestle for 30 min. The obtained MoS_2 powder was then dispersed into 10 mL NMP solvent. The slurry was then probe-sonicated (Ultrasonic Processor GEX500) for 24 h at 125 W sonication power and finally centrifuged for 20 min at 8000 rpm. The precipitate was dispersed in ethanol to obtain a supernatant containing 2D MoS_2 nanoflakes with a concentration of 3 mg mL^{-1}.

Preparation of PDA/MoS_2 films

PDA monomers, PCDA (10 mg), were dissolved in ethanol (1 mL) and filtered using a 0.45 μm PVDF filter (Millipore) to remove the pre-polymerized materials. The colorless PCDA solution with a concentration of 3 mg mL^{-1} was mixed with MoS_2 suspension followed by stirring for 30 min in the dark. The mass ratio of MoS_2 to PDA was varied from 0% to 20%. The solution was then spin-coated on a PET film to make a thin white film. Irradiation of the monomer film with a hand-held UV lamp (254 nm, 1 mW cm^{-2}, 10 min) resulted in the generation of a transparent and blue-colored film.

Gas-sensing measurements

The gas-sensing measurements were carried out using a WS-30A measuring system (Zhengzhou Winsen Electronics Technology, P. R. China). The DMF vapor with defined concentrations in the range of 0.01% to 4% was generated by dropping the corresponding amounts of DMF liquid onto a hot plate in the chamber. The temperature of the chamber was controlled at 25 ± 2 °C for eliminating the possible thermochromism for PDA (typically >40 °C).[14,15] The sensitivity of the sensor to methanol, THF, and acetone was also tested by using the same method to obtain the gas-sensing selectivity data. A quantitative measure for the blue-red color transition was given by the colorimetric response, which was defined as follows:

$$B_i = \frac{A_{\mathrm{Blue}}}{A_{\mathrm{Blue}} + A_{\mathrm{Red}}} \times 100\%$$

where A_{Blue} was the absorbance at ~640 nm and A_{Red} was the absorbance at ~550 nm. The B_i of the PDA/MoS_2 film in the

absence and presence of an organic vapor was recorded to calculate the vapor-induced colorimetric response (CR).

$$\mathrm{CR} = \frac{(B_0 - B_1)}{B_0} \times 100\%$$

where B_0 and B_1 were the percent of blue before and after organic vapor treatment, respectively.

General techniques

Scanning electron microscopy (SEM) images were obtained using a Zeiss Supra 55 instrument at a voltage of 20 kV. Fourier-transform infrared (FTIR) spectra were collected on a Nicolet 6700 FTIR spectrometer. Transmission electron microscopy (TEM) images were collected on JEOL 2100F equipment. UV-vis transmittance spectra were recorded by using a Shimadzu UV-2600 UV spectrophotometer.

Results and discussion

The typical procedures for the fabrication of a flexible transparent sensor based on PDA/MoS_2 films are schematically illustrated in Fig. 1. 2D MoS_2 flakes were firstly prepared from MoS_2 bulk powder using a grinding-assisted liquid-phase exfoliation technique in *N*-methyl-2-pyrrolidone (NMP) solution. The MoS_2 nanosheet suspension was added into PCDA monomer solutions followed by vigorous stirring to guarantee the full interaction and self-assembly of PCDA on MoS_2 nanosheets (PCDA/MoS_2) based on the chelation effect between the carboxyl group and MoS_2.[24,25,32] The composite was then spin-coated on a flexible and transparent PET substrate, yielding a transparent white film. After the illumination of UV light at a wavelength of 254 nm for 2 min, the PCDA/MoS_2 film was converted into a transparent blue film. The PDA/MoS_2 film can be used for selectively sensing DMF gas and the colorimetric response of the films was recorded after exposure to DMF gas.

Fig. 2 shows the photographs of PET (A), PCDA/MoS_2 on PET (B), and PDA/MoS_2 on PET (C and D) films. The composite

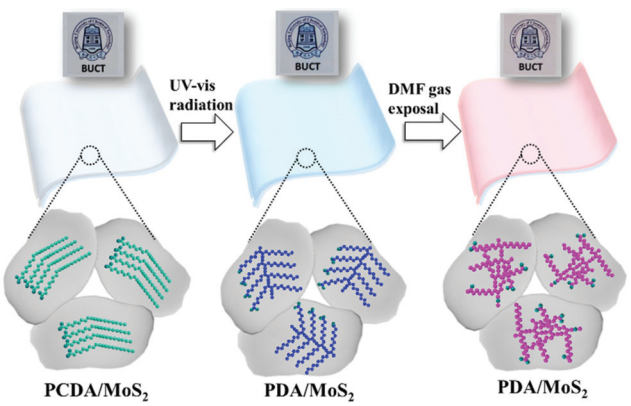

Fig. 1 Schematic illustration of the preparation of the PDA/MoS_2 film and the sensor upon exposure to DMF vapor.

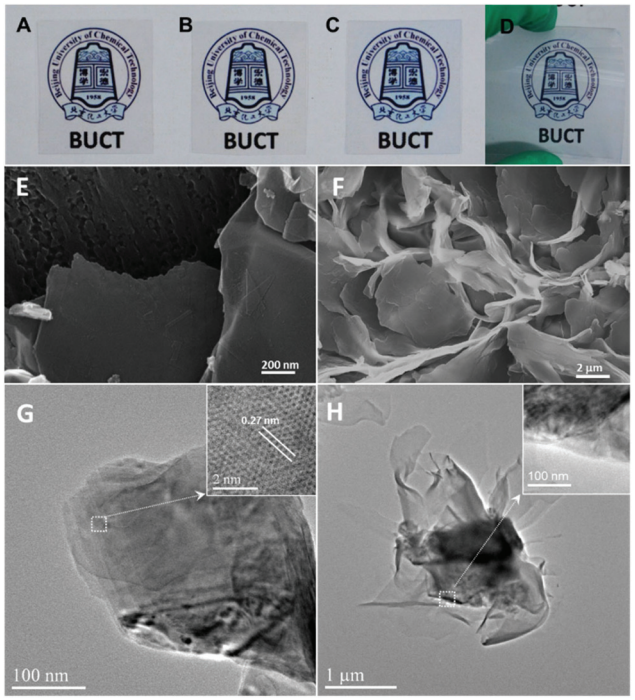

Fig. 2 Digital images of flexible and transparent PET (A), PCDA/MoS_2 on PET (B), and PDA/MoS_2 on PET (C and D) films. SEM and TEM images of MoS_2 (E and G) and PDA/MoS_2 (F and H).

was synthesized with a mass ratio of MoS_2 to PDA at 5%. The PCDA/MoS_2 film was transparent and white, and it was transformed to blue after illumination with UV light. This typical white to blue color change indicated the formation of PDA upon UV illumination. The digital images clearly showed the highly flexible and transparent properties of PDA/MoS_2 films. The micromorphology of MoS_2, PDA and PDA/MoS_2 films was further characterized by SEM and TEM techniques, as shown in Fig. 2 and S1.† The SEM image of MoS_2 in Fig. 2E shows that MoS_2 flakes with a nanosheet structure were obtained *via* the solvent exfoliation method. The SEM image of PDA/MoS_2 films in Fig. 2F reveals the random piles of nanosheets with flower-like and porous structures, which might favor the permeation of organic vapors and enhance the adsorption surface area for gas sensing application. Comparatively, PDA aggregation was observed in the absence of MoS_2 in the SEM image of PDA films in Fig. S1,† which might decrease lots of sensing sites and thus be adverse for gas sensing. The high-resolution transmission electron microscopy (HRTEM) image and fast Fourier transformation (FFT) pattern (Fig. S2A†) of MoS_2 confirmed the nanosheet structure with a typical crystalline order and a lattice fringe of 2.7 Å, corresponding to the (100) lattice of MoS_2.[33–35] As shown in the TEM image and FFT pattern of PDA/MoS_2 (Fig. 2H and S2†), an amorphous structure was observed on the crystalline flakes with flower-like morphology, indicating the formation of hierarchical PDA/MoS_2 composites. The elemental analysis of MoS_2 and PDA/MoS_2 in Fig. S3† indicated that both Mo and S elements were observed in MoS_2 and PDA/MoS_2 samples, and the peak intensity of the

C element was enhanced for the PDA/MoS_2 sample compared with that of MoS_2, which further proved the formation of PDA/MoS_2 composites.

The structures of MoS_2, PDA, and PDA/MoS_2 were then characterized by FTIR, as shown in Fig. S4.† The FTIR peaks in the range from 400 to 600 cm^{-1} for MoS_2 were ascribed to the sulfur-to-metal vibration.[36] The FTIR spectra of PDA molecules showed peaks of the carbonyl stretching band at 1694 cm^{-1}, symmetric methylene stretching at 2851 cm^{-1}, asymmetric methylene stretching at 2922 cm^{-1}, and hydroxyl stretching at 3433 cm^{-1}.[37] PDA/MoS_2 exhibited characteristic peaks of PDA while the peak of the carbonyl stretching band shifted from an initial value of 1694 to 1686 cm^{-1}, which should be due to the interaction between the carboxyl groups of PDA and MoS_2, namely the hydrogen bond of H to S and the chelation of O to the Mo center at defect sites in MoS_2 sheets.[24,32] Moreover, the MoS_2 absorbance peaks in the PDA/MoS_2 sample were not obvious due to the high peak intensity of PDA and the small concentrations of MoS_2 within the composite. The UV-vis spectra of all samples were also collected to confirm their structure, as shown in Fig. S5.† All the films exhibited a typical peak at ~640 nm, which was ascribed to the conjugated blue phase PDA supramolecule.[14] The magnification of the UV-vis spectra in Fig. S5B† showed a small peak shift from 637 to 643 nm with the ratio increase of MoS_2, which further confirmed the chelation of MoS_2 with the carboxyl groups of PDA.[24,25,32]

To display the effect of MoS_2 on the performance of films, the transmittance and gas sensing performance of films prepared with varied amounts of MoS_2 were investigated in detail. Fig. 3A shows that the transmittance of PDA/MoS_2 films with a mass ratio of MoS_2 to PDA varied as 0%, 2.5%, 5%, 10%, and 20%, which was denoted as PDA, PDA/MoS_2-1, PDA/MoS_2-2, PDA/MoS_2-3, and PDA/MoS_2-4, respectively. As the amount of MoS_2 increased in the films, the transmittance at 640 nm increased from 70% to 95%, indicating that the presence of MoS_2 enhanced the film transparency. The increased transparency should be ascribed to the following effects. The nanosheet structure of MoS_2 acted as scaffolds for PDA, which might favor the ordered assembly of PCDA and hinder the aggregation of PDA films *via* the interaction of MoS_2 and PDA. Moreover, the hydrophilicity of MoS_2 increased the affinity of films towards hydrophilic PET.[38] The decreased aggregation of PDA films and increased affinity toward the transparent PET substrate are beneficial for the formation of flexible transparent films. After exposure to DMF vapor, the transmittances of all samples were higher than 70% (Fig. S6†), indicating that the films kept high transparency during the detection process, which ensured the integration of sensors into electronics without adverse effects on the normal function of the electronic display screen.

The DMF-induced structure changes of polymers were investigated by UV-vis spectra in Fig. 3 and S7.† After exposure to DMF gas, the signal peak intensity at ~640 nm ascribed to the blue phase PDA was weakened and another adsorption peak at ~550 nm appeared, ascribed to the red phase PDA.[14] It has been proven that the blue and red colors of PDA were

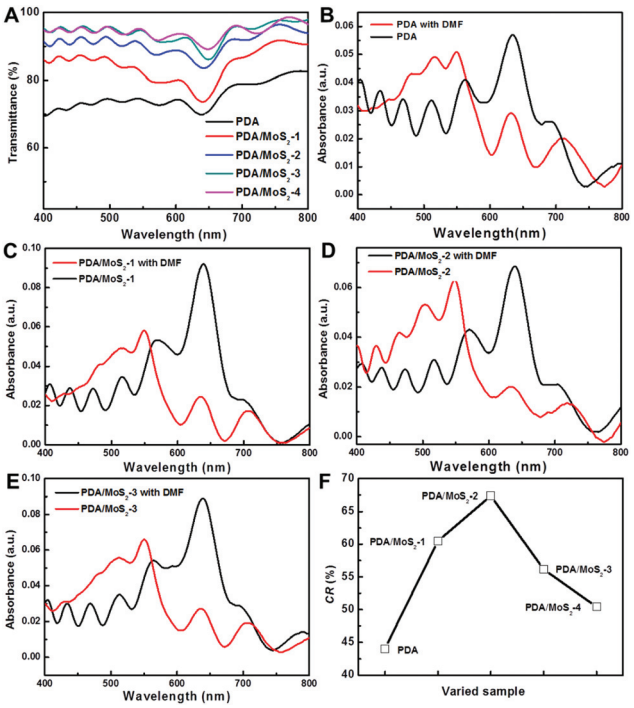

Fig. 3 Transmittance spectra of PDA, PDA/MoS_2-1, PDA/MoS_2-2, PDA/MoS_2-3, and PDA/MoS_2-4 films (A). UV-vis spectra of PDA/MoS_2 composites with an increased ratio of MoS_2 to PDA in the absence and presence of 0.1% DMF vapor (B, C, D, and E). The CR value of all the corresponding samples with different MoS_2 amounts upon exposure to 0.1% DMF (F).

greatly affected by the chain fluctuation. When the PDA composite films were exposed to organic vapors, the interaction of organic vapors with PDA led to the deformation of chains, contributing to the color change from blue to red.[14,17,39] The DMF-induced color change of the PDA/MoS_2 film was evaluated by quantifying the chromatic response (CR) according to the ratio of blue to red color before and after DMF treatment. The detailed calculation procedures are shown in the Experimental section. Fig. 3F shows the CR value of all the corresponding samples with different MoS_2 amounts upon exposure to 0.1% DMF. The increased CR value with the enhancement in the MoS_2 amount indicated that the presence of MoS_2 enhanced the gas sensing performance and the largest CR value was obtained for the optimal ratio of MoS_2 to PDA at 5%. The enhanced sensing performance should be ascribed to the flower-like composites with MoS_2 nanosheets as a scaffold and PDA as a coating layer, which possessed a porous structure and a high surface area, thus facilitating gas diffusion and increasing the gas sensing sites. On the other hand, further increasing the MoS_2 amount should lead to the overlap of MoS_2 on PDA and shield a part of reactive sites of PDA for gas sensing, which was adverse for sensing performance. Therefore, introducing an optimal amount of MoS_2 to PDA films enhanced the transparency and gas sensing performance due to the decreased aggregation, increased surface area and porosity.

The UV-vis spectra of PDA/MoS_2 films prepared *via* the optimal amount of MoS_2 were recorded when exposed to DMF vapor with different concentrations, as shown in Fig. 4A. As the DMF vapor concentration increased, the peak intensity at ~640 nm was gradually weakened, accompanied by the increased intensity of the adsorption peak at ~550 nm, indicating the microscopic "blue-to-red" chromatic phase transition of PDA materials.[17] The CR values of PDA/MoS_2 films exposed to DMF vapor with different volume concentrations were calculated as shown in Fig. 4B. There was a linear relationship between the CR value and the DMF concentration with R^2 of 0.958, namely CR = 20.73 × c_{DMF} + 3.78 in the vapor volume concentrations ranging from 0.01% to 4%. The mechanism for the blue to red chromatic change of PDA induced by an organic vapor is generally believed to be the dissolution of partially polymerized oligomers in common organic solvents, creating void in the PDA, which leads to partial distortion of the polymer backbone and a colour change.[14,17,39] In the presence of DMF vapor, the interaction of DMF and side chains of PDA in PDA/MoS_2 films due to the principle of similarity and intermiscibility led to the conjugated backbone twisting and side-chain fluctuations, synergistically contributing to the color change of PDA/MoS_2 films, as shown in Fig. 1. Exploiting the linear range, it is possible to quantitatively measure the concentration of DMF vapor. The digital images of PDA/MoS_2 films after vapor treatment showed the visible color change from blue to red with the DMF vapor concentrations in the range of 1%–4%, as shown in Fig. 4C. It is reported that long time exposure to 0.032% DMF and above could induce heart damage, which is in the linear detection range of the sensor developed here.[40] The explosive limits of DMF are from 2.2% to 16% v/v in air[41] and the sensor will give out a vivid color change signal once the concentration reaches 1%. The vivid color change observed in response to DMF vapor is one of the major advantages of the PDA-based chemical sensor system over those based on other conjugated polymers.

Sensor flexibility was tested by recording the sensing performance after 500 bending/extending cycles. As shown in Fig. 5A, the CR value did not exhibit any obvious changes at room temperature, revealing the reliability and excellent flexibility of this device. The sensing performance upon exposure to different vapors, including CH_3OH, $CHCl_3$, and THF is shown in Fig. 5B. The PDA/MoS_2 film displayed vivid color changes to red in DMF vapor while no obvious color changes were observed in other vapors, indicating that the PDA/MoS_2 film exhibited better selective detection sensitivity for DMF than other vapors. Compared with the reported PDA sensors with no selectivity toward DMF, it is rationally concluded that MoS_2 with a high affinity to nitrogen containing gas species favored the adsorption of DMF on the films and thus enhanced the selective sensor sensitivity to DMF.[29–31] Based on the high transparency, vivid color change detected by the naked eye, remarkable flexibility and reliability, wearable wrist strap sensor devices with visible DMF sensing ability based on PDA/MoS_2 films were fabricated, indicating their great potential for smart wearable devices, as shown in Fig. 5C. The visible, portable, and sensitive alarm for DMF vapor leakage possesses great potential and significance to monitor the safety of manufacture due to the extensive employment of DMF as an organic solvent in the manufacturing industry.

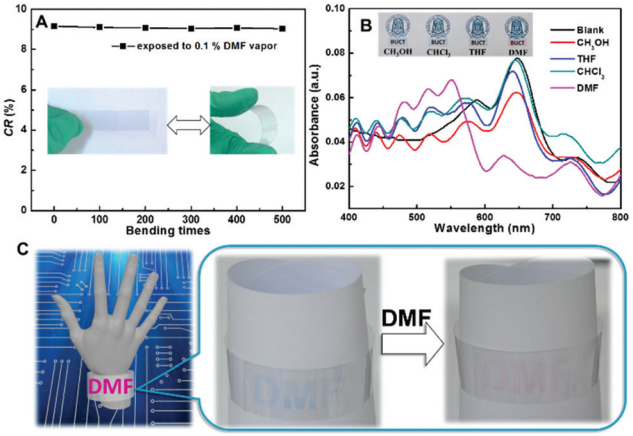

Fig. 5 Response of the PDA/MoS_2-PET film exposed to 0.1% DMF vapor after different bending times (A). UV-vis spectra of the PDA/MoS_2 film upon exposure to different (5%) vapors, in comparison with 2% DMF vapor (B). Flexible transparent wrist strap with DMF sensing ability (C).

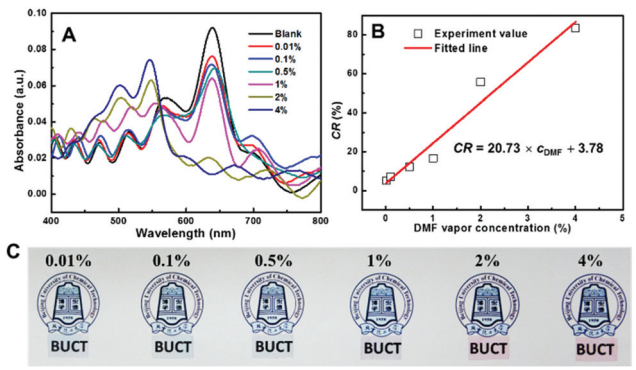

Fig. 4 UV-vis spectra (A), CR value (B), and (C) the digital images of PDA/MoS_2 films exposed to DMF vapor with different concentrations.

Conclusion

The present research developed a flexible, transparent, and portable DMF gas sensor based on hierarchical PDA/MoS_2 films. MoS_2 with a nanoflake structure supported and facilitated the formation of PDA films *via* the chelation interaction between MoS_2 and carboxyl groups of PDA. The introduction of MoS_2 increased the porosity and transparency of the films, which further enhanced the sensitivity, selectivity and application potential of the sensor. The PDA/MoS_2 film exhibited a linear chromatic response for DMF vapor with concentrations from 0.01% to 4%. A visible color change from blue to red was observed with a DMF gaseous concentration higher than 1%, which was more obvious than other organic vapor gases.

Based on PDA/MoS_2 films, a wearable wrist strap device with visible DMF sensing ability was fabricated, which indicated great potential for smart wearable devices by exploiting the high transparency, vivid color change detected by the naked eye, remarkable flexibility and reliability of PDA/MoS_2 films.

Acknowledgements

This work was financially supported by the China Postdoctoral Science Foundation Funded Project (2016M592518), the Natural Science Foundation of China (61435010, 61490713, 61675135, 21404006), the Science and Technology Innovation Commission of Shenzhen (KQTD2015032416270385 and JCYJ20150625103619275), the Beijing Natural Science Foundation (2152023), the National Key Research and Development Project (2016YFC0801302), and the Fundamental Research Funds for the Central Universities.

Notes and references

1 D. J. Lipomi, M. Vosgueritchian, B. C.-K. Tee, S. L. Hellstrom, J. A. Lee, C. H. Fox and Z. Bao, *Nat. Nanotechnol.*, 2011, **6**, 788–792.
2 C. Liao, M. Zhang, M. Y. Yao, T. Hua, L. Li and F. Yan, *Adv. Mater.*, 2015, **27**, 7493–7527.
3 W. Gao, S. Emaminejad, H. Y. Y. Nyein, S. Challa, K. Chen, A. Peck, H. M. Fahad, H. Ota, H. Shiraki, D. Kiriya, D.-H. Lien, G. A. Brooks, R. W. Davis and A. Javey, *Nature*, 2016, **529**, 509–514.
4 Z. Zhang, D. S. Kim, C.-Y. Lin, H. Zhang, A. D. Lammer, V. M. Lynch, I. Popov, O. Š. Miljanić, E. V. Anslyn and J. L. Sessler, *J. Am. Chem. Soc.*, 2015, **137**, 7769–7774.
5 T. Wang, Y. Guo, P. Wan, H. Zhang, X. Chen and X. Sun, *Small*, 2016, **12**, 3748–3756.
6 S.-Y. Cho, Y. Lee, H.-J. Koh, H. Jung, J.-S. Kim, H. W. Yoo, J. Kim and H.-T. Jung, *Adv. Mater.*, 2016, **28**, 7020–7028.
7 X. Zhou, S. Lee, Z. Xu and J. Yoon, *Chem. Rev.*, 2015, **115**, 7944.
8 H. Liu, M. Li, O. Voznyy, L. Hu, Q. Fu, D. Zhou, Z. Xia, E. H. Sargent and J. Tang, *Adv. Mater.*, 2014, **26**, 2718–2724.
9 S. Ammu, V. Dua, S. R. Agnihotra, S. P. Surwade, A. Phulgirkar, S. Patel and S. K. Manohar, *J. Am. Chem. Soc.*, 2012, **134**, 4553–4556.
10 S. Bai, C. Sun, P. Wan, C. Wang, R. Luo, Y. Li, J. Liu and X. Sun, *Small*, 2015, **11**, 306–310.
11 A. Kaushik, R. Kumar, S. K. Arya, M. Nair, B. D. Malhotra and S. Bhansali, *Chem. Rev.*, 2015, **115**, 4571–4606.
12 L. Feng, C. Zhu, H. Yuan, L. Liu, F. Lv and S. Wang, *Chem. Soc. Rev.*, 2013, **42**, 6620–6633.
13 X. Chen, G. Zhou, X. Peng and J. Yoon, *Chem. Soc. Rev.*, 2012, **41**, 4610–4630.
14 J. Lee, M. Pyo, S.-H. Lee, J. Kim, M. Ra, W.-Y. Kim, B. J. Park, C. W. Lee and J.-M. Kim, *Nat. Commun.*, 2014, **5**, 3736.
15 D.-H. Park, J. Hong, I. S. Park, C. W. Lee and J.-M. Kim, *Adv. Funct. Mater.*, 2014, **24**, 5186–5193.
16 S.-H. Jung, H. Jang, M.-C. Lim, J. H. Kim, K.-S. Shin, S. M. Kim, H.-Y. Kim, Y. R. Kim and T.-J. Jeon, *Anal. Chem.*, 2015, **87**, 2072–2078.
17 X. Wang, X. Sun, P. A. Hu, J. Zhang, L. Wang, W. Feng, S. Lei, B. Yang and W. Cao, *Adv. Funct. Mater.*, 2013, **23**, 6044–6050.
18 K. S. Novoselov, A. K. Geim, S. Morozov, D. Jiang, Y. Zhang, S. A. Dubonos, I. Grigorieva and A. Firsov, *Science*, 2004, **306**, 666–669.
19 K. S. Kim, Y. Zhao, H. Jang, S. Y. Lee, J. M. Kim, K. S. Kim, J.-H. Ahn, P. Kim, J.-Y. Choi and B. H. Hong, *Nature*, 2009, **457**, 706–710.
20 G. R. Bhimanapati, Z. Lin, V. Meunier, Y. Jung, J. Cha, S. Das, D. Xiao, Y. Son, M. S. Strano and V. R. Cooper, *ACS Nano*, 2015, **9**, 11509–11539.
21 H. P. Cong, J. F. Chen and S. H. Yu, *Chem. Soc. Rev.*, 2014, **43**, 7295–7325.
22 P. P. Wang, H. Sun, Y. Ji, W. Li and X. Wang, *Adv. Mater.*, 2014, **26**, 964–969.
23 X. Huang, Z. Zeng and H. Zhang, *Chem. Soc. Rev.*, 2013, **42**, 1934–1946.
24 H. Tang, J. Wang, H. Yin, H. Zhao, D. Wang and Z. Tang, *Adv. Mater.*, 2015, **27**, 1117–1123.
25 J. Zhu, W. Sun, D. Yang, Y. Zhang, H. H. Hoon, H. Zhang and Q. Yan, *Small*, 2015, **11**, 4123–4129.
26 G. L. Kennedy, *Crit. Rev. Toxicol.*, 2012, **42**, 793–826.
27 X. Chen, J. Zhao, J. Zhao, Y. He, L. Wang and Z. Bao, *Int. Biodeterior. Biodegrad.*, 2015, **104**, 435–442.
28 Y. Li, S. Zhang and D. Song, *Angew. Chem., Int. Ed.*, 2013, **125**, 738–741.
29 F. K. Perkins, A. L. Friedman, E. Cobas, P. Campbell, G. Jernigan and B. T. Jonker, *Nano Lett.*, 2013, **13**, 668–673.
30 B. Liu, L. Chen, G. Liu, A. N. Abbas, M. Fathi and C. Zhou, *ACS Nano*, 2014, **8**, 5304–5314.
31 Q. He, Z. Zeng, Z. Yin, H. Li, S. Wu, X. Huang and H. Zhang, *Small*, 2012, **8**, 2994–2999.
32 J.-S. Kim, H.-W. Yoo, H. O. Choi and H.-T. Jung, *Nano Lett.*, 2014, **14**, 5941–5947.
33 J. Brivio, D. T. Alexander and A. Kis, *Nano Lett.*, 2011, **11**, 5148–5153.
34 L. Yang, S. Wang, J. Mao, J. Deng, Q. Gao, Y. Tang and O. G. Schmidt, *Adv. Mater.*, 2013, **25**, 1180–1184.
35 D. Gao, M. Si, J. Li, J. Zhang, Z. Zhang, Z. Yang and D. Xue, *Nanoscale Res. Lett.*, 2013, **8**, 129.
36 X. Geng, W. Sun, W. Wu, B. Chen, A. Al Hilo, M. Benamara, H. Zhu, F. Watanabe, J. Cui and T. P. Chen, *Nat. Commun.*, 2016, **7**, 10672.
37 J.-M. Kim, J.-S. Lee, H. Choi, D. Sohn and D. J. Ahn, *Macromolecules*, 2005, **38**, 9366–9376.
38 Y. Li, C. Y. Xu and L. Zhen, *Appl. Phys. Lett.*, 2013, **102**, 143110.
39 J. Lee, S. Seo and J. Kim, *Adv. Funct. Mater.*, 2012, **22**, 1632–1638.
40 D. Rui, C. Daojun and Y. Yongjian, *Environ. Toxicol. Pharmacol.*, 2011, **31**, 357–363.
41 M. Khamforoush and T. Asgari, *Nano*, 2015, **10**, 1550016.

